https://doi.org/10.48047/AFJBS.6.13.2024. 232-263

African Journal of Biological Sciences

Potential for overpowering drug resistance in MCF-7/Adr cells by regulation of apoptotic pathways using sorafenib that incorporates chitosan-conjugated folic acid nanoparticles: An Experimental Study

Asmaa Hassan [1], Ahmed Nabil [1*], Islam S. Ali [2], Mariam Elwan [3], Zeinab Reyd [4], Osama M. Ahmed [5], Ahmed A. G. El-Shahawy [4]

[1] Biotechnology and Life Sciences Department, Faculty of Postgraduate Studies for Advanced Sciences (PSAS), Beni-Suef University, Beni-Suef, Egypt.

[2] Basic Science Department, Delta University for Science and Technology, Gamasa, Dakahlia, Egypt.

[3] Egyptian Ministry of Health, Mansoura, Dakahlia, Egypt.

[4] Materials Science and Nanotechnology Department, Faculty of Postgraduate Studies for Advanced Sciences (PSAS), Beni-Suef University, Beni-Suef, Egypt.

[5] Physiology Division, Faculty of Science, Beni-Suef University, Beni-Suef, Egypt.

***Corresponding author:**

Ahmed Nabil, Biotechnology and Life Sciences Department, Faculty of Postgraduate Studies for Advanced Sciences (PSAS), Beni-Suef University, Beni-Suef, Egypt,

E-mail: DRNABIL_100@hotmail.com

Tel: (+2) 01000618349

Graphical Abstract:

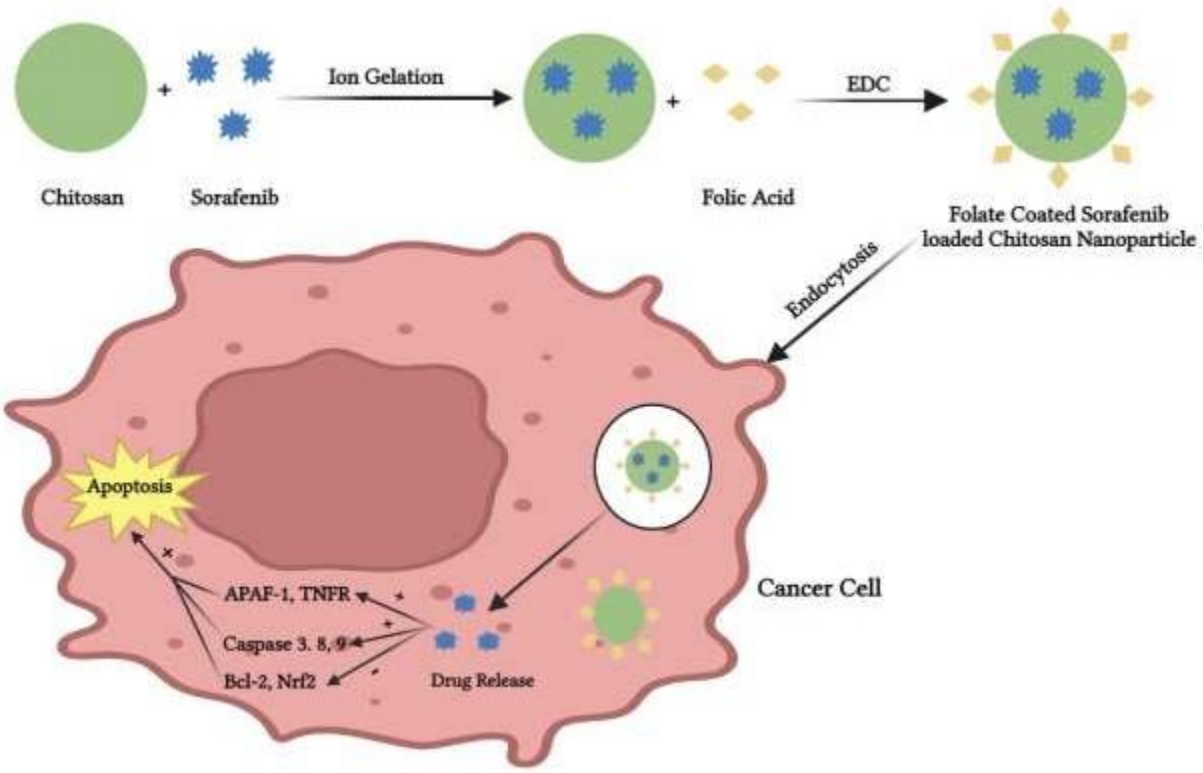

Article History
Volume 6, Issue 13, 2024
Received: 18June 2024
Accepted: 02July 2024
doi:***10.48047/AFJBS.6.13.2024.232-263***

Abstract:

This study aims to develop a novel formulation of chitosan-sorafenib-conjugated folic acid nanoparticles to overcome drug resistance and induce apoptosis in human breast cancer cell line. A drug release experiment was performed, and the loading capacity and entrapment efficiency were estimated. The combined nanoformula was tested as an anticancer treatment against breast cancer cells by a flowcytometry assay, cell cycle analysis, DNA fragmentation assay, quantitative real-time polymerase chain reaction, and Western blot. Furthermore, DNA fragmentation results indicate that this novel nanoformula caused higher apoptosis data. Inhibition of cell cycle progression was also higher with this combined nanoformula. Up-regulation of caspase 3, caspase 8 and caspase 9, cytochrome c was also observed; in contrast, the expression of the antiapoptotic marker B-cell lymphoma-2 was reduced in the combined nanoformula treated group compared to their individual treatments. Therefore, this combined nanoformula can improve the survival rate of patients with breast cancer.

Keywords: breast cancer, Sorafenib, chitosan, tumor targeting, apoptosis, overcome multidrug resistance.

1. Introduction:

Breast cancer is the most prevalent type of cancer among women (Fraguas-Sánchez et al. 2020). There are three main cancer treatment strategies: surgery, radiotherapy, and chemotherapy. Many chemotherapeutic agents have been allowed for the treatment of breast cancer, depending on the receptors that are expressed. These drugs differ in their mode of action and can be combined with a hormonal therapeutic agent such as tamoxifen. However, chemotherapy treatment is still limited due to low bioavailability, high dose requirements, low therapeutic indices, adverse side effects, nonspecific targeting, and drug resistance (Waks and Winer 2019; Tran et al. 2020).

Sorafenib (Sor) is a multikinase inhibitor that targets tyrosine kinase receptors such as the Vascular Endothelial Growth Factor Receptor (VEGFR) 1, 2, and 3, as well as Fms-like tyrosine kinase-3 (Flt-3) and a tyrosine kinase receptor called c-Kit. These kinases are involved in signaling, proliferation, angiogenesis, and apoptosis of tumor cells. Furthermore, Sor inhibits intracellular Raf serine/threonine kinases in the Mitogen-activated protein kinase (MAPK) cascade (Fumarola et al. 2013; Truong et al. 2015; Keating 2017). Previous preclinical studies have shown that sorafenib is effective in slowing tumor progression for hepatocellular, colon, renal, pancreatic, ovarian, thyroid, and breast cancer. However, sorafenib monotherapy still has a low tumor response and side effects (Wilhelm et al. 2018), revealing the need to improve sorafenib efficiency and decrease its toxicity.

Nanodelivery systems have high efficiency in drug loading, encapsulation, intracellular absorption, controlled release, and finally accumulation in cancer cells. As a result, these systems are in high demand in the clinical stage. Therefore, more efficient nanocarriers are required to achieve the mentioned goals and overcome chemotherapy side effects (Senapati et al. 2018). Chitin, the main component of crustacean shells, can be deacetylated to create chitosan (Cs). 1-4 linked D-glucosamine and N-Acetyl-D-glucosamine form the linear polysaccharide chain that forms Cs (Shanmuganathan et al. 2019). Studies have demonstrated the exceptional qualities of Cs nanoparticles, which include safety, biodegradability, nonimmunogenicity, extended blood circulation time, improved drug stability, the capacity for controlled and sustained release of the drug, and biocompatibility for targeting the drug at the cellular level (Chae et al. 2005; Khan et al. 2017).

Folic acid (FA), commonly known as vitamin B9, is crucial for cell proliferation. Cancer cells require a sufficient supply of folate, so several cancer cells attempt to overexpress the folate receptors on their surface to significantly uptake additional FA in competition with their surrounding cells (Shahverdi et al. 2018; Nguyen et al. 2019). In addition, FA has low toxicity and immunogenicity and a high affinity for the folate receptor, which is overexpressed in cancer cells (Li et al. 2015). Therefore, the decoration of nanomaterials with this folate enhances their uptake and efficacy against tumors, in addition to decreasing their cytotoxicity against other non-cancerous cells. The main statement of the problem is that the MCF7/Adr breast cancer cell line has multidrug resistance due to the overexpression of drug efflux "pump" proteins, which mediate drug efflux of several chemotherapeutic drugs and reduce intracellular drug accumulation, leading to poor responses to many conventional chemo-drugs and cancer recurrence (Li et al. 2018). This study aims to develop a sorafenib formulation containing chitosan-conjugated folic

acid to achieve active targeting that overcomes multidrug resistance (MDR) by activating apoptosis signaling pathways in breast cancer cells. We refer to this formula as "combination" throughout the manuscript.

2. Materials and methods:

2.1. Materials:

Fetal bovine serum (FBS), Dulbecco's modified Eagle medium (DMEM), and 0.25% trypsin / EDTA (200 mg / ml of EDTA, 170,000 U of Trypsin L-1) were obtained from Lonza, Belgium. Antibiotics and antimitotics (penicillin and streptomycin), Trypan Blue 0.4%, and the MTT test kit were purchased from Lonza, USA. Kreps-Ringer bicarbonate buffer (Sigma-Aldrich, USA), bovine serum albumin (BSA) solution and 1X phosphate buffered saline (PBS) (Hyclone, USA) Sorafenib was obtained from Bayer Pharma (Müller Strasse, Berlin, Germany). Antibodies against P53, B-cell lymphoma-2 protein (Bcl-2), caspase 3, and caspase 9 were obtained from BD Biosciences. Caspase-8 antibodies were obtained from Thermo Fisher Scientific. Analytical grade and high purity were employed for all chemicals and solvents.

2.2. Methods:

2.2.1. Preparation of Sor in nanoparticles

Sorafenib was prepared by dissolving 0.02 g of Sorafenib in 10 ml of ethanol and stirring for 15 min. 0.45 g of polyphosphoric acid (PPA) was dissolved in 75 ml of distilled water and 25 ml of ethanol, which was stirred for 10 min. The sorafenib solution was added dropwise with a syringe to the PPA solution and sonicated for 10 min. The resulting sorafenib particle suspension was cooled by centrifuging it for 30 minutes at 7000 rpm with a lypholizer.

2.2.2. Preparation of Cs nanoparticles (CsNPs) (Ionic gelation method):

Using sodium tripolyphosphate (TPP) to cause the gelation of a Cs solution, the Cs nanoparticles were produced. Positively charged amino groups and negatively charged TPP interact, forming ionotropic gelation. 0.2 g of chitosan was dissolved in 2 ml of Acetic acid and 100 ml of dist. H2O was stirred at room temperature with a magnetic stirrer until a clear solution was obtained. The Cs solution was brought to pH 4.8 to 5 with 1N NaOH. 0.0666 g of TPP was dissolved in 33.3 ml of distilled water to form a TPP solution. A magnetic stirrer was used to stir the chitosan solution at 800 rpm, while the TPP solution was added dropwise using a syringe at room temperature (RT) in the 3:1 ratio (v / v) (chitosan) (John et al. 2017). Sonication was performed for 20 min. The resulting suspension of Cs particles was cooled, centrifuged at 12,000 rpm for 30 minutes, and lyophilized to achieve both the best stability of the nanoparticles' characteristics and the best drug protection.

2.2.3. Preparation of Sor-loaded CsNPs:

For this purpose, 0.2 g of chitosan was dissolved in 2 ml of 1% CH_3COOH and 100 ml of deionized H_2O and stirred at RT with a magnetic stirrer until a clear solution formed. The chitosan solution was adjusted to pH 4.8 to 5 with 1N NaOH. Sor was prepared by dissolving 0.01 g of Sor in 10 ml of acetone. Sor-loaded CsNPs have been prepared by adding sor to a Cs solution under constant stirring. To make a TPP solution, dissolve 0.066 g of TPP in 33.3 ml of deionized water. The Sor-CsNP solution was stirred at 800 rpm, while the TPP solution was added drop by drop using

a syringe at RT. Sonication for 20 minutes, centrifugation at 7000 rpm for 30 minutes, and lyophilization for 30 minutes.

2.2.4. Preparation of sorafenib incorporating chitosan-conjugated folic acid nanoparticles (CsNPs-Sor-FA):

The same procedures were followed until the Sor-CsNP solution was obtained. After 2 hours of sonication, the solution was homogenized before dropping FA (0.1 g) droplets into a Sor-CsNP solution and stirring for 24 hours. Sonication for 20 minutes, centrifugation at 7000 rpm for 30 minutes, and lyophilization for 30 minutes

2.2.5. Characterizations of sorafenib incorporating chitosan-conjugated folic acid nanoparticles:

2.2.5.1. X-ray diffraction (XRD):

The instrument (PANalytical Empyrean) was operated with a 30 mA current, a 40 kV voltage, a scanning speed (2 / min) and a scanning range of 10 to 70. The size of the crystallite was estimated from the peaks of the XRD using the following equation:

$$D = 0.94\lambda/\beta \cos\theta \quad \text{(Eq. 1).}$$

Where D: the mean size of the crystallite, λ: the wavelength of the radiation, β: the corrected full width at 1/2 of the maximum diffraction, and θ: the diffraction angle.

2.2.5.2. Fourier transform-infrared spectroscopy (FT-IR):

The chemical structures of the prepared formula were investigated using an FT-IR spectrometer (Alpha II, Bruker). The samples were compacted into discs that could be scanned in the spectral range of 4000-500 cm1 after being combined with a spectroscopic grade of potassium bromide.

2.2.5.3. High-Resolution Transmission Electron Microscopy (HRTEM):

The morphology of the formula CsNPs-Sor-FA (combination) was detected by HRTEM (Jeol JEM-100S transmission electron microscope (TEM), Japan). The sample was dispersed in ethanol by sonication at 25 ° C for 15 min, diluted with ethanol (<0.01 wt.%), stained with phosphotungstic acid before spotting on carbon-coated copper grids and allowed to dry before testing. The diameter was assessed using Image J software. Data are presented as the mean ± standard deviation.

2.2.5.4. Entrapment Efficiency (EE):

The efficiency of Sor capture was evaluated using the UV spectrophotometry technique (Guido and Joseph 1992), using a UV-Vis spectrometer device (CAR100, Germany) to estimate the amount of free Sor at λ max = 265.5 nm (Li et al. 2019). The supernatant was separated from the sample of nanoformula by centrifugation at 4 °C and 14,000 rpm for 45 minutes. Free Sor in the supernatant was evaluated in triplicate (n = 3), and the Sor EE% was calculated using the following equation:

$$\text{EE \%} = \frac{(\text{Total amount of Sor} - \text{free amount of Sor})}{\text{Total amount of Sor}} \text{X100} \quad \text{(Eq. 2)}.$$

2.2.5.5. Sorafenib release study:

The dialysis bag technique was used to study Sor release as a free Sor from CsNPs-Sor and the CsNPs-Sor-FA formula using a molecular weight cutoff of cellophane membranes at 10,000 to 12,000 Dalton (Tamilselvan and Raghavan 2015). (0.1 g) CsNPs-Sor-FA is the weight at the start of the study, which is equivalent to 20 mg of Sor. The starting weight was transformed into a suspension (5 ml) and placed inside a dialysis bag. The neck of the bag was then sealed and the bag was placed in 200 ml of phosphate buffer (pH 6.8) to mimic the acidic environment of cancer cells. The assembly was placed in a shaking incubator set at 37 degrees Celsius and 150 rpm. The samples were dragged and equaled an equivalent volume of fresh buffer at different time periods. The sor concentration, which was released from the CsNP-Sor-FA formula, was estimated by a UV-vis spectrophotometer, as explained in the previous experiment. Also, the free Sor released was estimated under the same conditions as the control. The percentage of loaded capacity was computed as follows:

$$\%\text{Loading Capacity} = \frac{\text{Initial Sorafenib} - \text{Free Sorafenib}}{\text{CsNPs}-\text{Sor}-\text{FA}} \text{X}100 \quad (\text{Eq. } 3). \text{ (Ghosheh et al. 1999)}$$

2.2.5.6. Kinetics release of sorafenib from the CsNP-Sor-FA formula:

Data derived from the release examination were analyzed using kinetic models (eg, first order, zero order, Korsmeyer-Peppas, Higuchi and Hixson). The attained correlation coefficients (R2) were adjusted to the best-fit model. The drug release mechanism was delineated from the Peppas equation as follows:

$$\frac{\text{Mt}}{\text{M}\infty} = \text{Kt}^{\text{n}} \quad (\text{Eq. } 5)$$

Where Mt denotes the amount of drug released during time t, M refers to the total amount of drug released at infinity, K represents the release constant rate, and "n" represents the Peppas diffusion exponent, demonstrating the method of drug release and the kind of diffusion (Wang et al. 2015).

2.2.6. Cell culture:

Human breast cancer MCF7/Adr cells and normal WI-38 cell lines (human lung fibroblast) were purchased from VACSERA, Egypt. Cells were cultured in DMEM medium, supplemented with penicillin (100 mg/ml), streptomycin (100 mg/ml), and fetal bovine serum (FBS) (10% v/v). Cells were kept at 37 ° C in an incubator with humidity of 5% CO2.

2.2.7. MTT Assay:

MCF7/Adr cells were seeded at a density of 6000 cells/well and incubated for 24 hours in growth medium to allow the cells to adhere to the wells. The medium was removed, and the cells were incubated with several concentrations of test substances (sorafenib, nanosorafenib, and nanoparticle combinations) dissolved in dimethyl sulfoxide (DMSO). The treated cells were incubated for 24 hours under the same conditions, then the medium was removed, and MTT solution (100 µl) was added and incubated for 3 hours. Then 50 µl of DMSO was added to dissolve the purple crystals and the plate was incubated for 15 minutes. The absorbance was measured at 570 nm. Cisplatin (Hospira UK Ltd.) was used as a control. This test was carried out in triplicate. IC50 and SI were calculated (Abdel-Motaal and Nabil 2018).

2.2.8. Evaluation of apoptosis:

Flow cytometry using the Accuri C6 version (Accuri C6-BD) was used to assess P53, caspase 9, caspase 3, caspase 8, and Bcl-2. Cells were treated with sorafenib, nanosorafenib, and combination CsNPs-Sor-FA and dissolved in DMEM medium for 48 hours, harvested by trypsinization, and centrifuged in fresh medium for 5 min. The supernatant was removed, and the pellet was added to a fresh medium. 100 µl of cell suspension was washed with PBS/BSA and centrifuged for 5 min. The supernatant was removed, and the pellet was added to PBS, then 10 µl of each marker (P53, caspase 9, caspase 8, caspase 3, and Bcl-2) was added and thoroughly mixed, and the tubes were incubated at RT in the dark for 30 min. To remove unbound antibodies, cells were washed with PBS or BSA, centrifuged for 5 minutes, and the supernatant was removed. Finally, cells were added to paraformaldehyde (4%) and then fixed until analysis by flow cytometry. The analysis of the markers P53, caspase 9, caspase 8, caspase 3, and Bcl-2 by flow cytometry was performed in triplicate. Also, annexin V/propidium iodide staining is used to assess levels of apoptosis. Untreated cells serve as a negative control. MCF-7/Adr cells were collected and stained using Annexin V and PI/fluorescein isothiocyanate (FITC) and incubated at RT for 15 min in the dark. Cells were added to the binding buffer and examined by flow cytometry using the Accuri C6-BD version. This test was also done in triplicate.

2.2.9. Cell cycle analysis:

The treated cell suspension (100 µl) (1x106 cells/ml) was washed with PBS/BSA (2 ml) and centrifuged. The cell suspension was treated with PI (propidium iodide RNase) and incubated for one hour at 4 ° C in the dark. Finally, incubated cells were analyzed in triplicate using flow cytometry (Accuri C6-BD).

2.2.10. Western blot analysis:

To determine the effect of sorafenib, nanosorafenib and CsNPs-Sor-FA on the expression of cytochrome-c and nuclear factor erythroid 2-related factor 2 (Nrf2), MCF7/Adr cells were treated with the drugs for 48 hours. Then radioimmunoprecipitation assay (RIPA) buffer was used to collect and lyse the cells. On sodium dodecylsulfate polyacrylamide gel electrophoresis (SDS-PAGE) gels, the total proteins were separated and then transferred to poly (vinylidene fluoride) (PVDF) membranes. Specific primary and secondary antibodies were used to investigate the proteins and protein bands were detected with enhanced chemiluminescence kits using the Chemi Doc MP imager.

2.2.11. Quantitative real-time PCR (qRT -PCR):

48-hour treated MCF7 / Adr cells were lysed for RNA isolation using the Qiagen extraction kit (Qiagen, USA). CDNA was produced from total RNA using a high-capacity cDNA reverse transcription kit (Fermentas, USA). Using an Applied Biosystem (version 3.1) (StepOneTM, USA), real-time qPCR amplification and analysis were carried out. The qPCR was catalyzed by SYBR Green Master (Qiagen, USA). PCR was carried out as follows: 50 ° C for 2 min, followed by 40 cycles for 15 sec at 95°C, 60 ° C for 1 min, and 72 ° C for 1 min. Data were analyzed and relative expression of the tumor necrosis factor receptor (TNFR) gene was calculated using the 2-Ct method. Each

measurement was made in triplicate. The PCR primer was purchased from Sino Biological Inc. (Cat# HP100759). The PCR primer sequences are shown in Table 1.

Table (1): PCR primer sequences for TNFR:

Gene Symbol	Primer sequence
TNFR	5'-CCATCTGCTGCACCAAGTGCCA-3' (F) 5'-AATCCTCGGTGGCAGTTACACA-3' (R)
Beta actin	5'-CACCATTGGCAATGAGCGGTTC-3' (F) 5'-AGGTCTTTGCGGATGTCCACGT-3' (R)

2.2.12. DNA fragmentation assay by electrophoresis:

MCF7/Adr cells were grown in cell culture (70% confluence) before treatment with sorafenib, nanosorafenib and CsNPs-Sor-FA for 48 h. DNA from the treated groups and the control group was extracted using the Qiagen kit (Qiagen, USA). DNA gel electrophoresis was performed using a 0.5% agarose gel. The bands were visualized under UV light. This test was carried out in triplicate.

2.2.13. Morphology of MCF-7 / Adr cell apoptosis by transmission electron microscopy:

To observe the morphology of the apoptotic MCF-7 / Adr cells, a transmission electron microscope (TEM) was used. Approximately 106 MCF-7 cells were treated separately with Sorafenib, nano-Sorafenib, CsNPs-Sor-FA and control cells without treatment. The cells without treatment were centrifuged down to a pellet and washed twice with PBS. The cells were passed through a series of ethanol and acetone solutions. Ultrathin sections were cut and dyed twice with lead citrate and uranyl acetate. Japan's JEOL-JEM 1010 TEM was used to examine the samples (Amin et al. 2018).

2.2.14. Statistical Analysis

IBM® SPSS® Statistics (Version 25) was used for the statistical analysis. Data were presented as mean ± standard deviation, and data distribution was verified using Kolmogorov-Smirnov and Shapiro-Wilk tests to explore normality. For multiple-group comparisons, parametric data were analyzed using a one-way analysis of variance (ANOVA). In all tests, the significance level (P-value) was established at <0.05. IBM Corporation, New York, USA, and SPSS, Inc. are divisions of IBM.

3. Results:

3.1. XRD analysis:

Figure 1 shows the qualitative XRD analysis for Sor, Cs, CsNPs, CsNPs-Sor, and CsNPs-Sor-FA. The figure shows the crystal pattern of a pure Sor. The figure shows multidiffracted peaks that reflect abundant structure plans and numerous electron densities for its molecular formula, $C_{21}H_{16}ClF_3N_4O_3$, where high crystallinity is indicated by a

high signal intensity with a narrow width of the diffracted peaks. There is no splitting in the peaks, which endorses a single phase of Sor. Using Equation 1, the crystallite size of pure Sor was estimated to be 60.78 Å at the highest relative intensity of 100% and a d-spacing of 6.75 Å at 13.1^0. This result is identical to the result of Ebadi et al. 2020 (Ebadi et al. 2020). Low diffraction signal intensities were shown in the Cs XRD spectra, which means low Cs crystallinity. The expanded width of the diffracted peaks represented the small size of the crystallites. The computed crystallite size of pure Cs was 2.98442 based on Equation 1. The irregular arrangement of Cs chains can be seen in the CsNP XRD spectrum, showing a large diffuse hump peak at 20 ° C, which is a typical semicrystalline Cs fingerprint. The current study's findings agree with an old study (Prathima et al. 2020) that demonstrated that the TPP counterions cause cross-linking between Cs chains, leading to an opaque network structure that removed the Cs diffraction peaks and created that single floppy peak. The presence of a broad peak, on the other hand, meant a reduction in crystallite size, indicating a lower periodicity and a reduction in the ordering of HKL planes, i.e., a reduction in crystallinity (Matthews et al. 1985). Another explanation for the low degree of crystalline perfection is defects in the nucleation and growth rate of the crystals caused by the use of a polymer, such as Cs (Katz et al., 2000). The CsNP-Sor XRD spectrum shows well-defined signal diffraction intensities that reflect periodicity with the ordering of the HKL planes and the crystallinity of the formula. Most of the time, this diffraction pattern was closely related to that of the Sor, revealing that the structure and integrity of the Sor were well preserved. Concerning the crystallization property of CsNPs-Sor-FA, Figure 1 revealed no obvious prominent peaks in the diffraction patterns with low diffraction intensities of the signal that reflect less periodicity, low ordering of HKL planes, and low crystallinity of the formula. However, two peaks were detected at 2 thetas 10.8o and 13.1o, indicating the presence of some crystallinity phase. Using Equation 1, the crystallite size of the formula was estimated to be 396.5 at the highest relative intensity of 100% with a d-spacing of 8.1 at 10.8o. In total, the CsNPs-Sor-FA spectrum shows hard mutations in the shape, diffracted signal position, and relative integrated intensity of the diffracted peaks over the range of diffraction. These alterations were shown to be interactions between Sor, CsNPs, and FA. The disordered crystalline phase of the formula was helpful for the sustained release of the Sor drug.

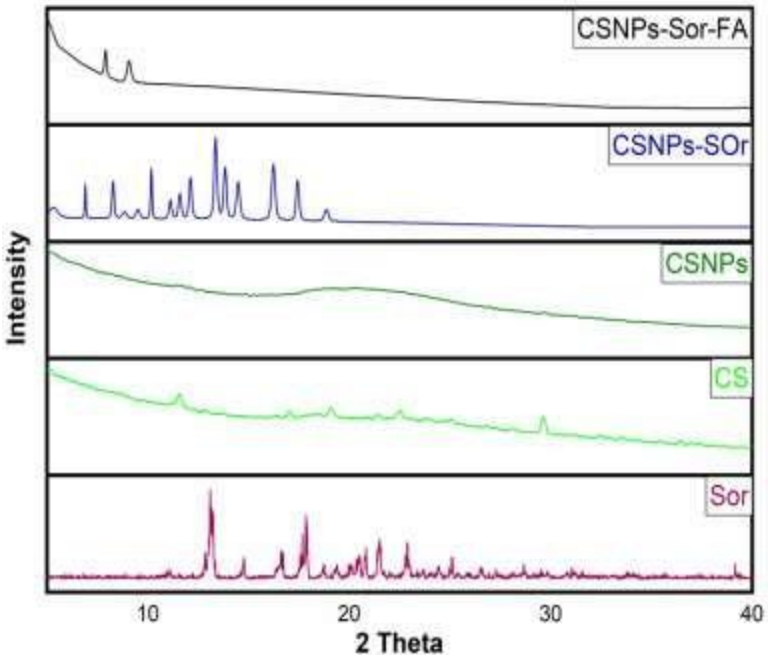

Figure 1. XRD of Sor, Cs, CsNPs, CsNPs-Sor, and CsNPs-Sor-FA. Over a 2θ range, the CsNPs-Sor spectrum showed languid changes in shape, position of the diffracted signals, and relative integrated intensity of the diffracted peaks, confirming Sor loading on CsNPs.

3.2. FTIR analysis:

Figure 2 shows the FTIR spectrum of Sor that appears to have multiple sharp, weak, and strong peaks; moreover, the pivotal functional groups match with CH, -CH2, -CH3, C = O, CO, N - H and C=C. The spectrum is compatible with the standard spectrum of solid Sor as well as with the previous study (Mittal et al. 2021). The spectrum appears to have a characteristic peak at 3120 cm-1 and 2930 cm^{-1} due to the C-H stretching bands of aromatic and aliphatic CH, respectively. The wave number 1512 cm^{-1} reveals the stretching band of the carbonyl group C=O. A weak C=C stretching peak (arrowhead) at 1640 cm^{-1} cannot be identified unambiguously. The stretching vibration peaks at 3733 cm-1 and 3671 cm^{-1} are attributed to N-H group primary amines. The weak peak at 1295 cm^{-1} reveals vibrations C–O–C. The expansion of alkene and aromatic sp2 C-H stretching vibrations appears at 1070 cm^{-1}. Exactly, the resulting spectrum reflects the molecular structure of Sor. Figure 2 also shows the FTIR spectrum of CsNPs as precursors. They showed numerous distinct peaks with small differences in broadness. The broad peak at 3419 cm^{-1} according to the chemical structure of Cs is due to the overlapping of O-H and N-H groups stretching vibrations. The width of this peak might be caused by hydrogen bond formation. The peaks are as follows: aliphatic C-H stretching at 2900 cm^{-1}, in-plane N-H bending vibration at 1662 cm^{-1}, primary alcoholic group C-O stretching vibration at 1414 cm^{-1}, and hydroxyl group C3-OH stretching vibration at 1098 cm^{-1} (Guido and Joseph 1992). The formula CsNPs-Sor-FA revealed a broad peak of the O-H group at 3432 cm-1, indicating the formation of hydrogen bonds between

the N-H and O-H groups of sorafenib, CsNPs, and FA. With reference to the carboxylic acid, side chain amide, and C=C groups, the FTIR spectra showed numerous major peaks of FA at 1694, 1646, and 1548 cm^{-1}, respectively. Significantly, the positions and patterns of peaks in the formula CsNPs-Sor-FA are distinct and completely different; furthermore, the peaks of the Sor disappeared, reflecting the Sor incorporation between CsNPs-Sor-FA, and this reverberated a type of interaction between Sor, CsNPs, and FA, which confirmed the synthesis of the formula.

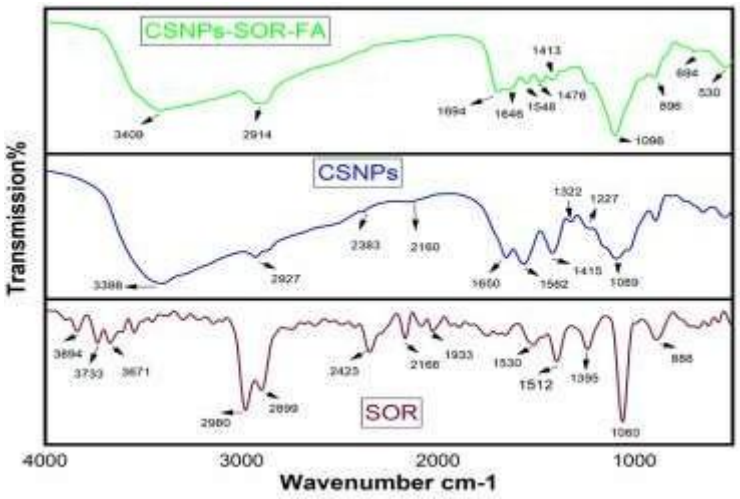

Figure 2. FTIR of Sor, CsNPs, and CsNPs-Sor. CsNPs-Sor peak patterns and positions varied significantly. These variations reflected the interaction between CsNPs and Sor, confirming the loading process.

3.3. Surface morphology (HRTEM study):

With respect to ultrastructural analysis, HRTEM is used to investigate the morphology of the prepared materials. Figure 3 shows HRTEM images of Sor (Figure 3A) and the formula CsNPs-Sor-FA (Figure 3B). Figure 3A shows an irregular spherical shape of Sor with a mean particle size of approximately 20nm, revealing the tendency of the particles to form aggregates. Figure 3B, with a low field of view, revealed the aggregated semispherical and spherical shapes of the synthesized CsNPs-Sor-FA with particle sizes averaging around 60 nm and presented a heterogeneous morphology with an irregular particle size distribution. The figure exhibited the fusion of Sor particles in the matrix of CsNPs and was decorated with FA particles on the surface (dark dot, red arrowhead). Additionally, the images displayed varied signal intensities that might be related to the fluctuating weakening of the incident electron beam over CsNPs-Sor-FA. This attenuation depends on the electron densities of CsNPs, Sor, and FA, which approve the loading operation. The formation of CsNPs-Sor-FA may occur via intermolecular linkages between the hydroxyl groups of Sor and the amino groups of CsNPs and FA during the polymerization process or through electrostatic reactions between cationic and anionic molecules, such as CsNPs, FA, and Sor molecules, respectively. This behavior is largely governed by the chemical and physical criteria of the CsNP cargo molecules, FA, and Sor. Figure 3C presents the selected area of electron diffraction. The SEAD image revealed only one bright signal intensity due to the incident

of the electron beam on the surface of the formula, indicating its low crystallinity, and this was well matched with the XRD spectrum of the CsNPs-Sor-FA formula.

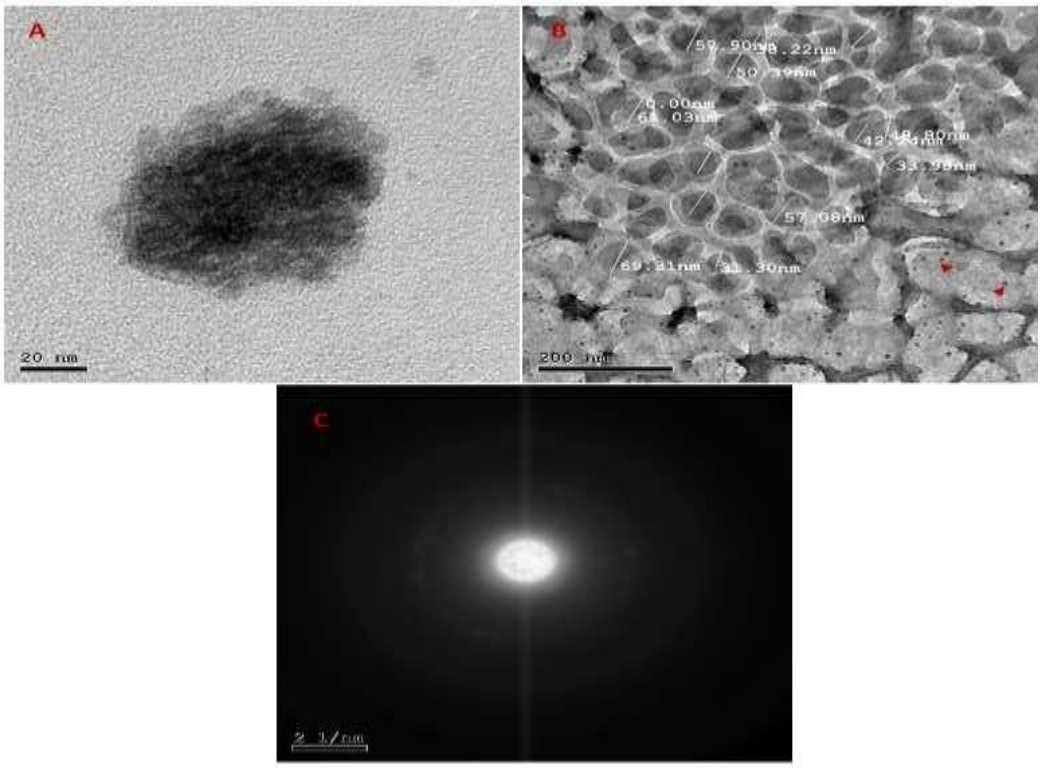

Figure 3. For the HRTEM images of (A) Sor and (B) CsNPs-Sor-FA, two distinct signal intensities were visible in the images, which could be attributed to variations in incident electron beam attenuation on CsNPs-Sor. And (C) SEAD image of CsNPs-Sor-FA, revealing a low crystallinity of the formula.

3.4. Entrapment efficiency and release study:

Equations 2 and 3 are used to calculate the EE and LC% for Sor, and the average results are 79± 2.9% and 13.6±1.2 %, respectively. Figure 4 shows the form of free Sor release in PBS solution over 120 hours and the profile of Sor release from the CsNPs-Sor-FA formula. The results indicate that Sor releases in two phases: a comparatively rapid burst release within the first 2 hours, followed by a characteristic slow-release rate up to 80 hours, reflecting a continuous-release phase. In the first 2 hours, 22.9% of the free Sor was released in a rapid burst, compared to only 16% of the CsNPs-Sor and 14% of the CsNPs-Sor-FA formula that were released in a minimal burst. The free Sor appears to release more quickly than the CsNPs-Sor and CsNPs-Sor-FA formulas. Free Sor has noncumulative particles, otherwise known as the CsNPs-Sor-FA formula, which refers to the interaction of Sor with CsNPs and FA; hence, Sor takes a long time to separate the interactions. The suggested interaction is via hydrogen bonding between the terminal group of the hydroxyl group (OH) of Sor, the functional amino group (NH2) of the CsNPs, and that of FA. After 80 hours, approximately 98% of free Sor is released, while only 82% of the CsNPs-Sor and about 77% of the CsNPs-Sor-FA formula are released in a sustained pattern. Sor release was sustained from CsNPs-Sor and CsNPs-Sor-FA up to 120 h, recording 90% and 88%, respectively, indicating that the CsNPs-Sor-FA formula has the potential

to control and sustain the release of Sor. In this research, we define the release order by conducting a release kinetic study. The kinetic analysis of the released Sor from the prepared formula of CsNPs-Sor-FA was conducted.

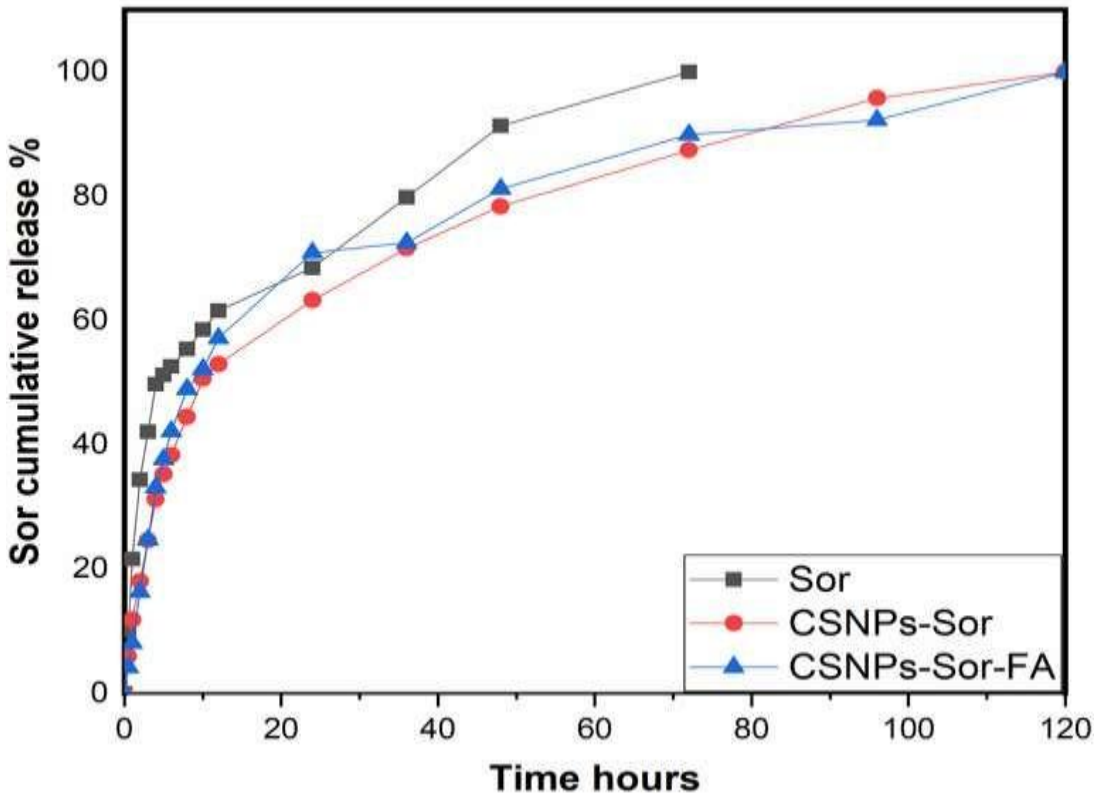

Figure 4. In vitro release profile of CsNPs-Sor compared to free Sor for 24 h at pH 6.8 and 37 ° C. The results are mean ± SEM (n = 3). Due to the slow diffusion of Sor from the CsNPs matrix, free Sor had a lower cumulative drug percentage than CsNPs-Sor, confirming a pattern of sustained release.

The kinetic Sor release data was fitted with four equations (Hixson-Crowell, Korsmeyer-Peppas, first-order equation, zero-order equation, Higuchi, and Hixson-Crowell), as shown in Figure 5. The Sor release mechanism was through the diffusion mechanism and followed the kinetic model with the maximum correlation coefficient value (R2) and a highly optimized Hixson model.

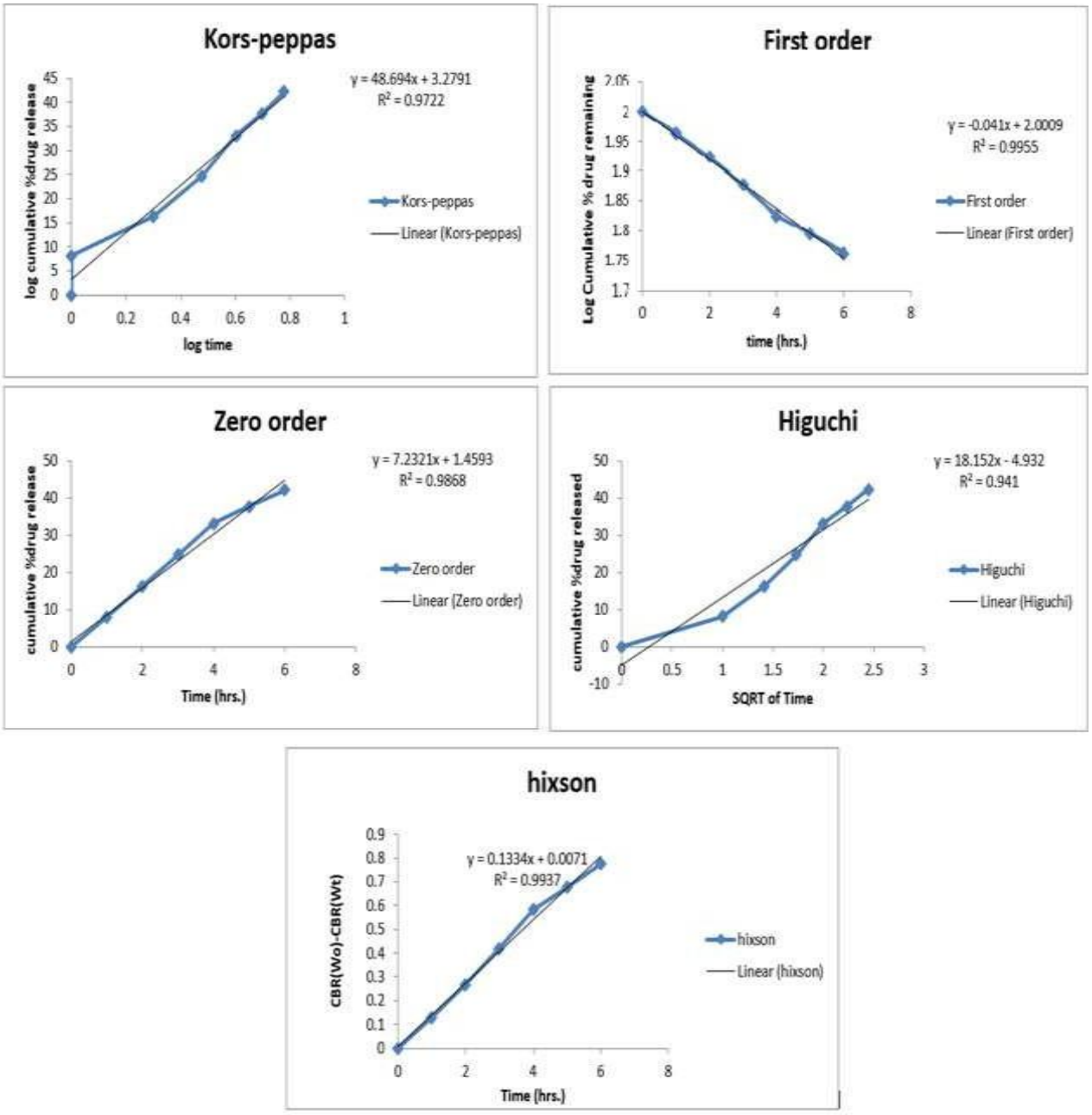

Figure 5. The kinetic Sor release data according to zero-order equation, first-order equation, Korsmeyer–Peppas, Hixson–Crowell, and Higuchi the Sor were released using diffusion with a highly best-fitting Hixson model.

3.5. Anticancer Activity:

The in vitro anticancer activity of various drugs was assessed against the MCF-7/Adr cell line. According to Table 2, Nano Sorafenib demonstrated the superior anticancer activity against MCF-7/Adr cell lines; with an IC50 value of 10 M, it was shown to be significantly more active than the sorafenib drug and the CsNPs-Sor-FA formula,

which had IC50 values of 15 M and 25 M, respectively. Sorafenib with chitosan demonstrated moderate cytotoxic activity, with an IC50 of 75 M. Cs showing negligible cytotoxicity. On the other hand, folic acid stimulates the proliferation of the MCF-7/Adr cell line. Therefore, from the above results, it is clear that three drugs (Sor, nano-Sor and the CsNPs-Sor-FA formula) exerted a strong anticancer effect against MCF-7/Adr breast cancer cells. By comparing a **drug's** cytotoxic impact on human lung fibroblasts in the normal WI-38 cell line with its cytotoxic impact on cancer cell lines, the selectivity index (SI) for sorafenib, nanosorafenib, and the CsNPs-Sor-FA formula was estimated. It was found that the sorafenib combination showed the most satisfactory selectivity index.

Table 2. The IC_{50} values of different drugs against MCF-7/Adr breast cancer cells and the selectivity index (SI) for Sor, nano-Sor, and CsNPs-Sor-FA:

Treatments	IC50 concentration against MCF-7/Adr cell line	IC_{50} concentration against WI-38 human normal cell line lung fibroblasts	SI
FA	Folic acid stimulates the proliferation of MCF-7/Adr cell line	-	-
Cs	>100 Mm	-	
CS-Sor	75 Mm	-	-
CsNPs-Sor-FA	25 Mm	>100 Mm	>4
Sor	15 Mm	25 Mm	1.6
Nano-Sor	10 Mm	15 Mm	1.5

3.6. Effect of sorafenib, nano-sorafenib, and the CsNPs-Sor-FA formula on apoptosis of MCF7/Adr cells:

As shown in Figures 6 and Figure 7, the highest expression of the anti-apoptotic Bcl-2 protein and the lowest expression of the apoptotic p53 protein and the caspase 3, 8, and 9 proteins were observed in untreated cells, which were employed as controls. In contrast to Sor or nano-Sor, the combination group significantly reduced anti-apoptotic Bcl-2 protein expression while increasing apoptotic proteins p53 and caspase 3, 8, and 9. Additionally, apoptotic cells were double labeled with annexin V-FITC and PI. In Figure 8A, the fluorescence sign areas of LL, LR, UR, and UL correspond to viable, early apoptosis, late apoptosis, and necrosis, respectively. As indicated by the statistical analysis in Figure 8B, the amounts of cell apoptosis and necrosis steadily increased from the Sor treatment group to the combination group. Compared to the control-treated group, the amount of late apoptosis and necrosis in MCF7/Adr cells increased significantly with Sor, nano-Sor, and combined treatment.

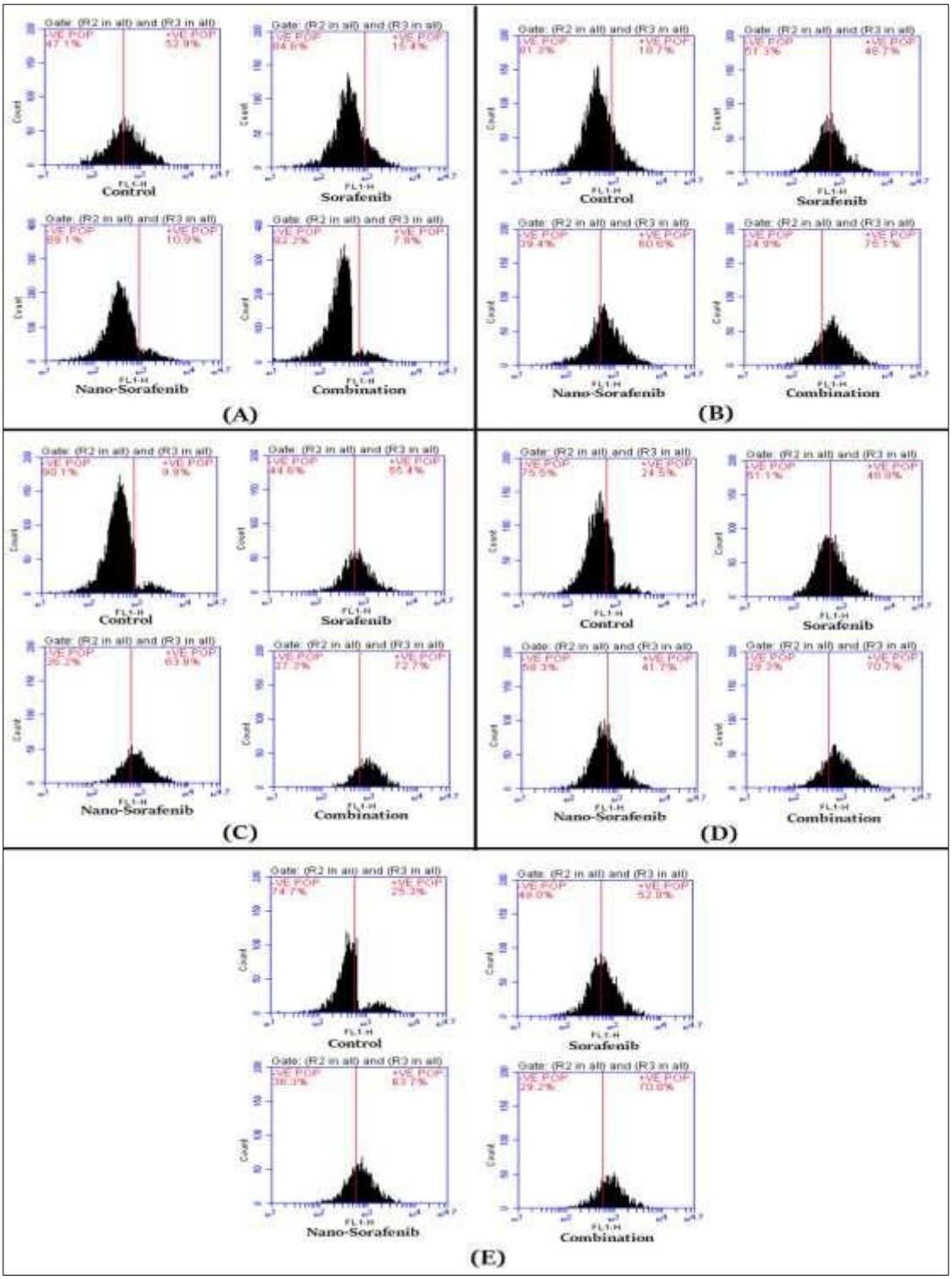

Figure 6. FCM histograms of Bcl-2(A), p53 (B) and caspase 3 (C), caspase 8 (D) and caspase 9 (E) in MCF-7/Adr cells with different treatment groups.

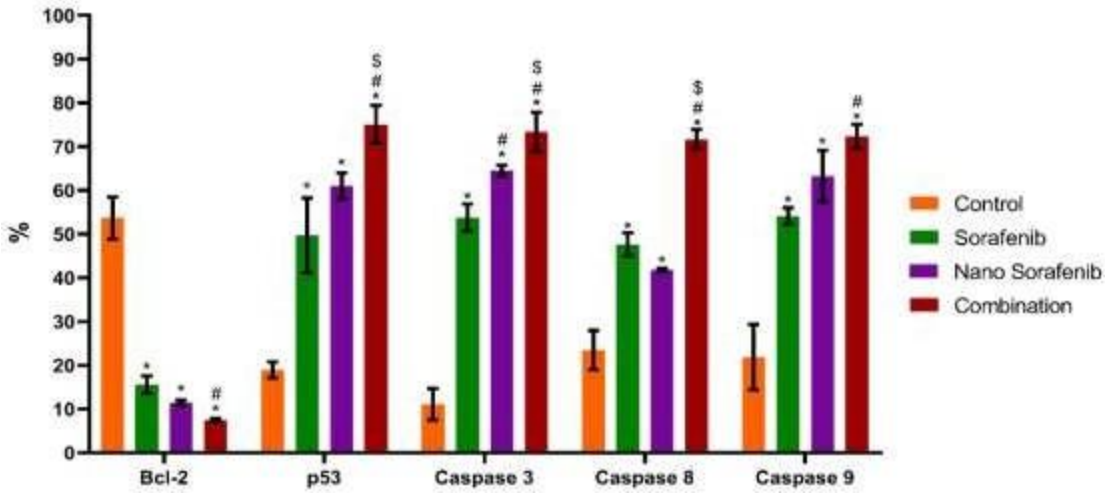

Figure 7. FCM analysis of Bcl-2, p53, and caspase 3, 8, 9 in MCF-7/Adr cells with different treatment groups. *: significant with the control group, #: significant with Sor group, $: significant with nano-Sor group.

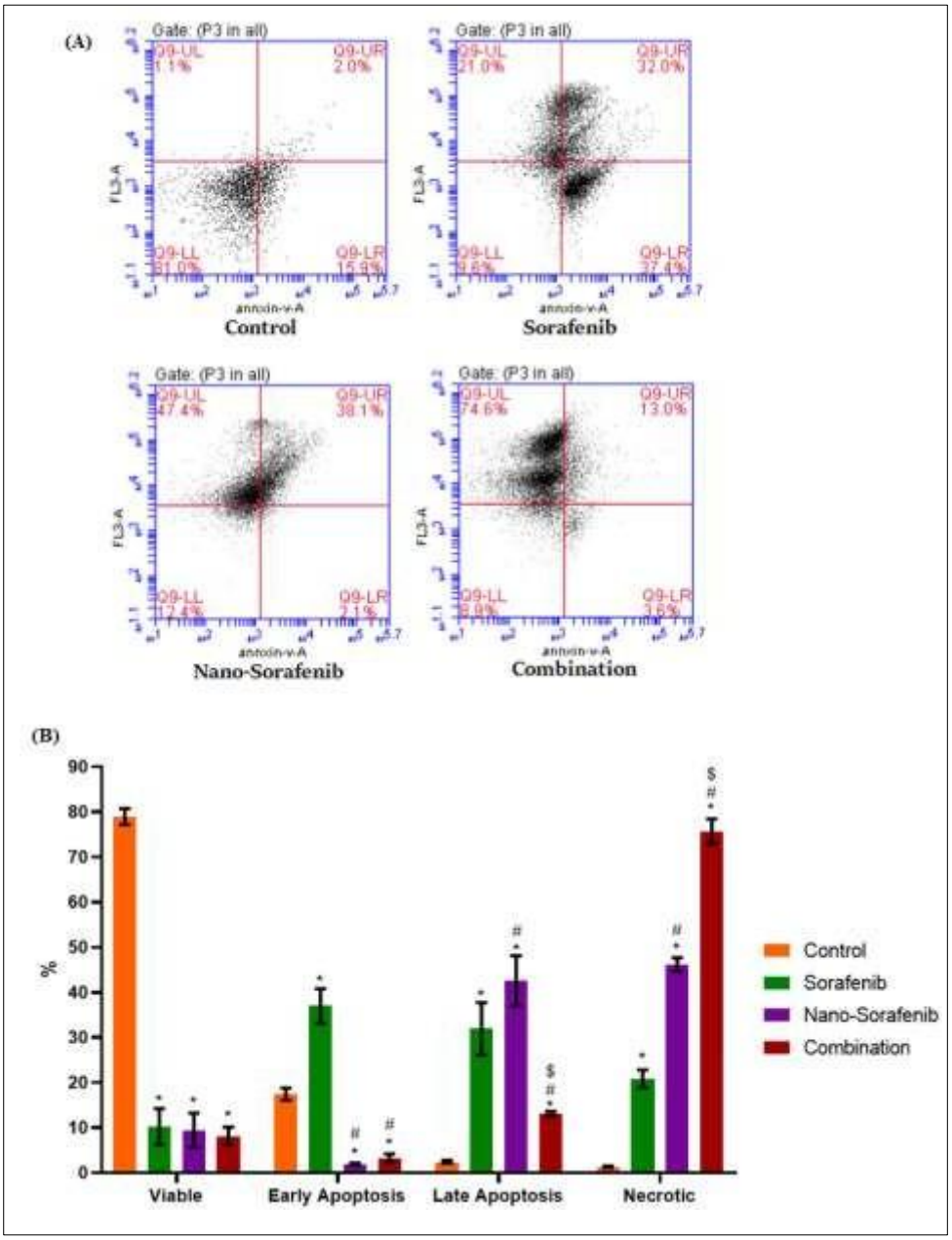

Figure 8. (A) FCM histogram of Annexin-V staining in MCF-7/Adr cells with different treatment groups. (B) FCM analysis of Annexin V staining in MCF-7/Adr cells with different treatment groups. *: significant with the control group, #: significant with Sor group, $: significant with nano-Sor group.

3.7. Effect of sorafenib, nano-sorafenib, and the CsNPs-Sor-FA formula on the cell cycle of MCF7/Adr cells:

The anticancer effects of nano-Sor, Sor, and the combination on the progression of the cell cycle were determined by using FCM because cell cycle progression is crucial for the proliferation of cancer cells. As shown in Figure 9, the results revealed that 5 percent of untreated control MCF7/Adr cells were in the sub-G1 phase, 72% were in the G0 phase, 26.43% were in the S phase and 2.47% were in the G2/M phase. Sor showed 12.97% for the sub-G1 phase, 72.93% for the G0 phase, 13.57% for synthesis, and 1.43% for the G2/M phase. Nano-Sor showed 14.67% for

the sub-G1 phase, 74.07% for the G0 phase, 11.4% for synthesis, and 0.77% for the G2/M phase. Our combination form had the most potent anticancer effect, reducing the S phase to 10.57% and blocking 1.07% of the cell population in the G2/M phase. As a result, we can conclude that the combination has a significant inhibitory effect on the MCF7/Adr cell line.

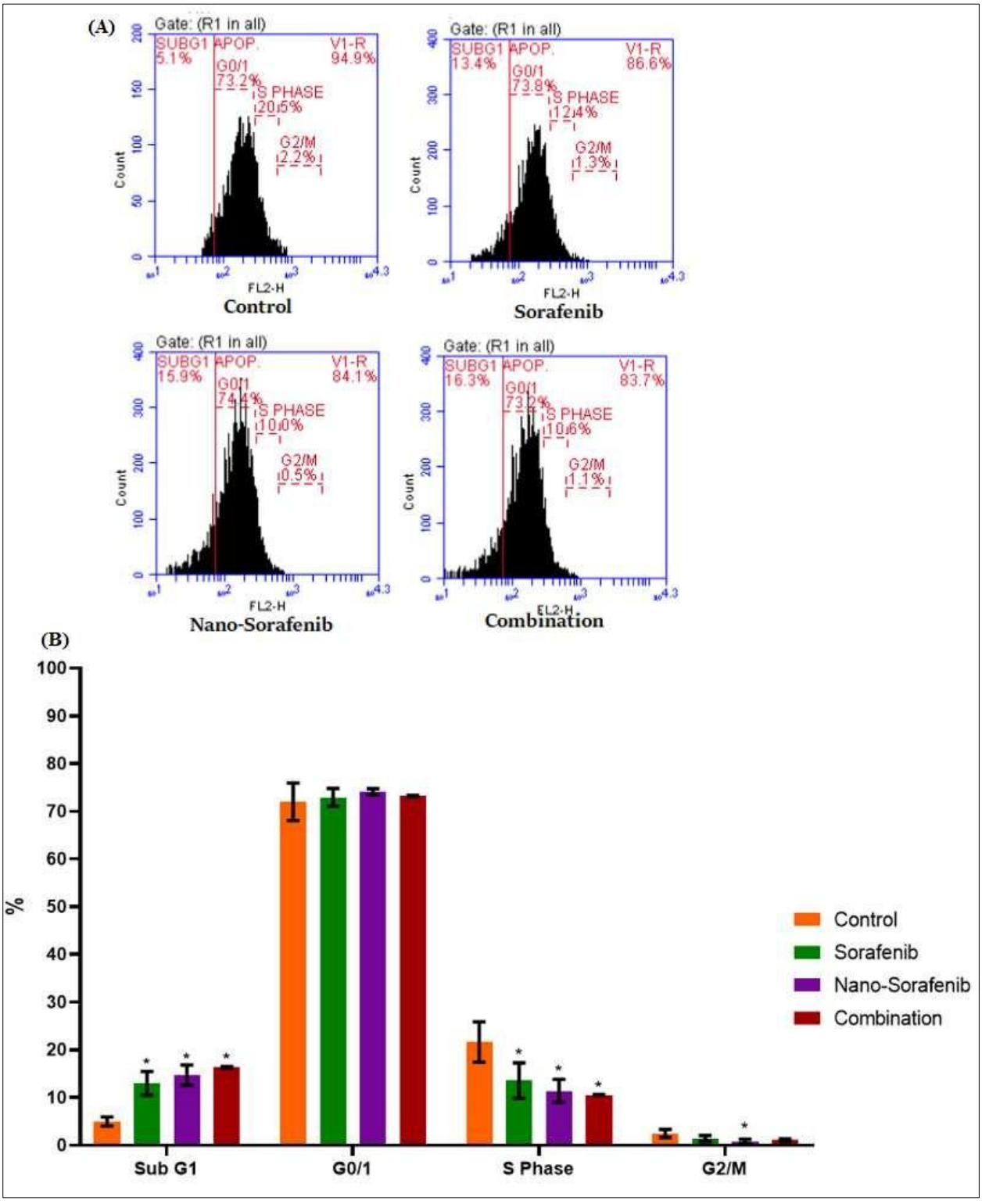

Figure 9. (A) Cell cycle histogram of MCF-7/Adr cells with different treatment groups. (B) Cell cycle analysis of MCF-7/Adr cells with different treatment groups. *: significant with the control group, #: significant with Sor group, $: significant with nano-Sor group.

3.8. Western blot analysis of Cytochrome-c and Nrf2:

When cytochrome c is released from mitochondria into the cytoplasm, DNA damage triggers apoptosis. To investigate the results of Cytochrome C in treated cells, we performed a Western blot analysis in the cytosol fraction. The intensity of the band (Figure 10A), and the statistical analysis (Figure 10B) showed that the expression of Cytochrome-c was slightly increased when cells were treated with Sor and nano-Sor. Furthermore, cytochrome c expression was highest in cells treated with combinations versus controls. This finding suggests that the combination, more than Sor and nano-Sor, induced apoptosis in MCF7/Adr cells through a cytochrome-c-dependent pathway. On the contrary, the Western blot analysis data (Figure 10A and B) showed that Nrf2 expression decreased significantly in the Sor, nano-Sor and combination groups compared to the control group.

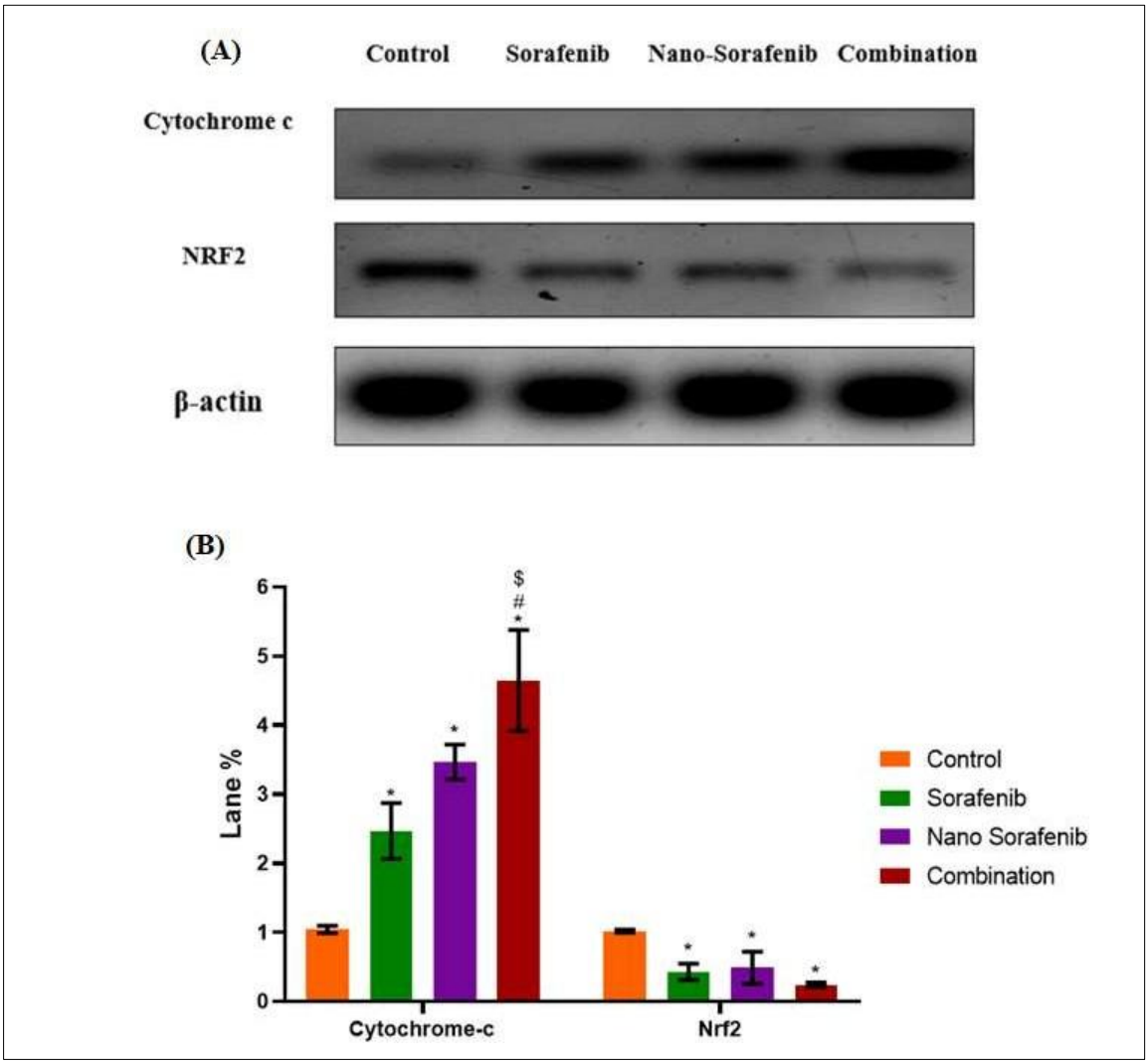

Figure 10. (A) Western blot bands of β-actin, Cytochrome-c, and Nrf2 in MCF-7/Adr cells with different treatment groups. (B) Western blot analysis of Cytochrome-c and Nrf2 in MCF-7/Adr cells with different treatment groups. *: significant with the control group, #: significant with Sor group, $: significant with nano-Sor group.

3.9. Effect of Sorafenib, nano-Sorafenib and combination on the mRNA level of TNFR:

TNFR is a cell membrane receptor that acts as a communication pathway to activate extrinsic cell death and apoptosis by binding to TNF. RT-PCR analyzes of TNFR mRNA expression in MCF7/A, MCF-7/Adr cell lines after exposure to sorafenib, nanosorafenib, and combinations showed that the expression of TNFR mRNA was highest in cells treated with combinations compared to their individual treatments (Figure 11).

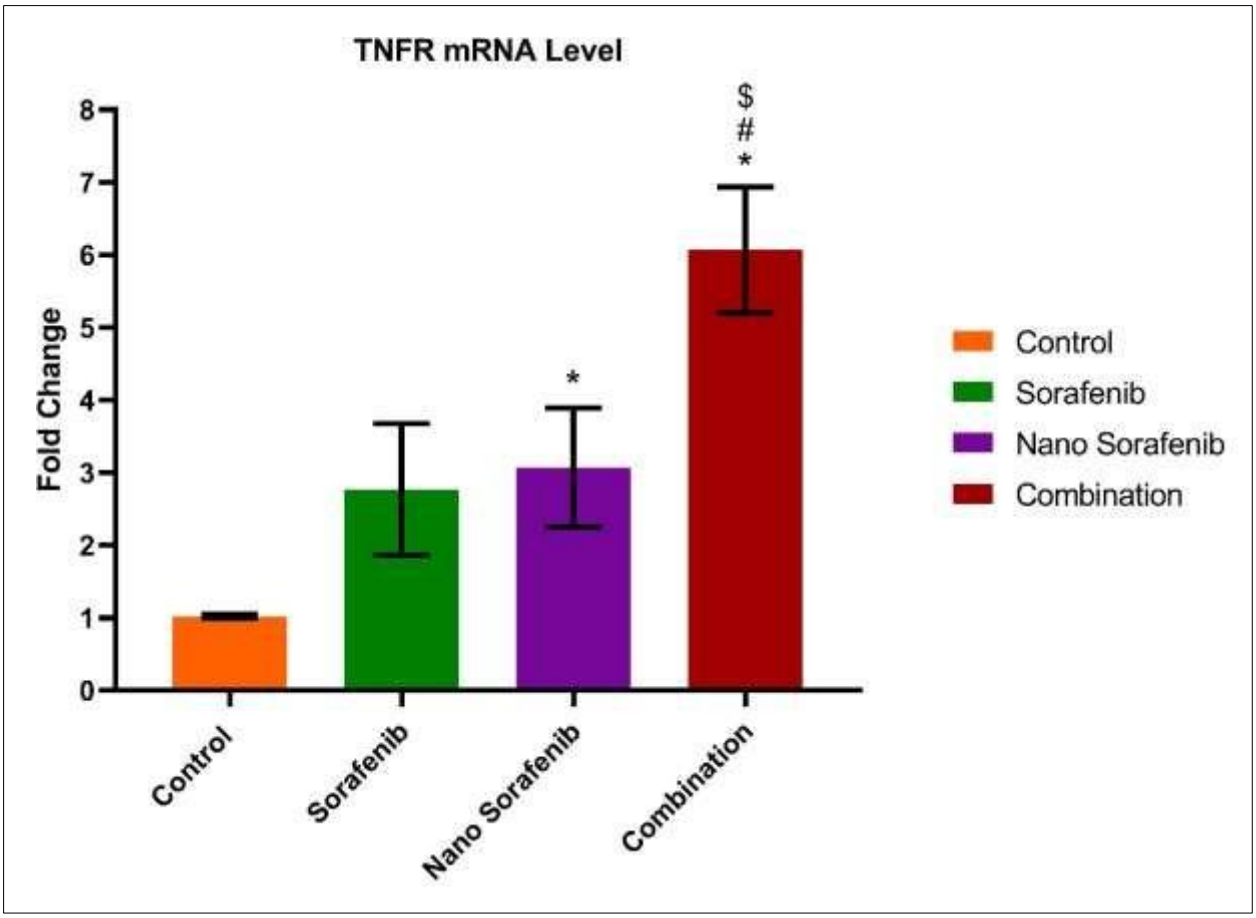

Figure 11. Effect of Sor, nano-Sor, and combination on TNFR mRNA levels in MCF-7 / Adr cell lines. *: significant with the control group, #: significant with Sor group, $: significant with nano-Sor group.

3.10. DNA fragmentation assay:

The study of DNA fragmentation was carried out using agarose gel electrophoresis. Compared to DNA markers, DNA fragments moved in different bands, making a ladder of approximately 100-1000 base pairs. Such DNA ladders are considered a hallmark of apoptosis and necrosis. In the present study, DNA bands from the control sample were intact and DNA fragments were not detected, as shown in Figure 12A. As shown in the figure, DNA fragmentation was detected and gradually increased in cells treated with sorafenib, nanosorafenib, and combinations. As a result, in Figure 12B, the combination induces high MCF7/Adr-induced DNA fragmentation, confirming the necrosis cell death mechanism and matching the results of annexin V-FITC.

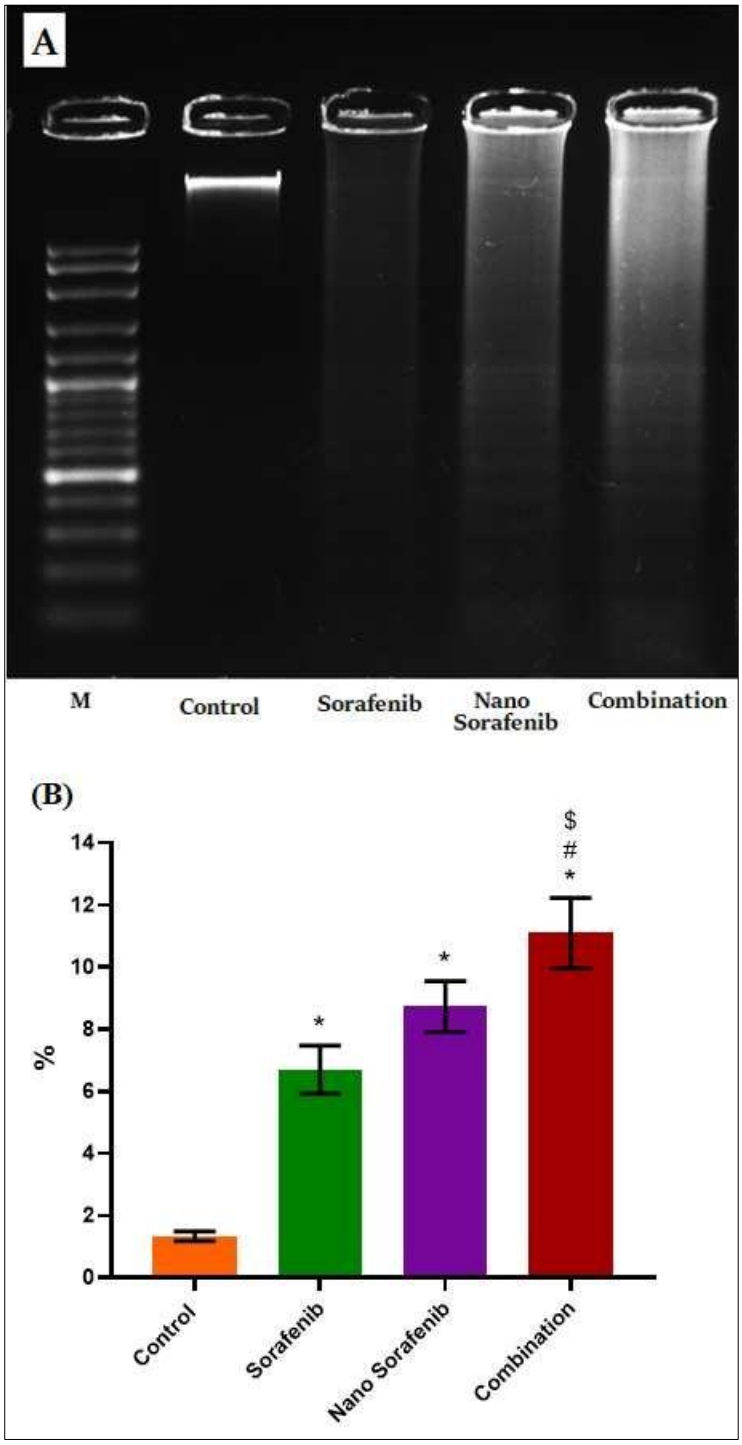

Figure 12. (A) Agarose gel electrophoresis of MCF7/Adr cell genomic DNA (DNA fragmentation) after treatment with Sor, nano-Sor and combination. (B) Statistical analysis of DNA fragmentation among the studied groups. *: significant with the control group, #: significant with Sor group, $: significant with nano-Sor group.

3.11. Transmission electron microscopy of the breast cancer cell line MCF-7/Adr treated with Sorafenib, nano-Sorafenib, and Combination:

The transmission electron microscope showed that the attached MCF-7/Adr cells in the control groups have multiple plasma cell membrane extensions and numerous microvilli. Furthermore, the cytoplasmic distribution of cellular organelles is distributed homogeneously (Figure 13A). Electron microscopy revealed apoptosis in floating cells but not in attached cells in the treated groups. Bio-TEM imaging revealed that MCF-7 / Adr cells were characterized by smoothing of the plasma membrane, elimination of microvilli, formation of intracytoplasmic vacuoles, rounding of the nucleus, and condensation of chromatin after exposure to sorafenib (Figure 13B). This was the phenomenon of early cell apoptosis. More nanocomplexes enter MCF-7 / Adr cells in the nano-Sor group, increasing cell apoptosis. In the Bio-TEM imaging nano Sor, vesicles phagocytosis increased, apoptotic cell separation of the apoptotic bodies disappeared, microvilli disappeared and condensed chromatin and a well-defined cell membrane emerged, indicating that the apoptosis of MCF-7 / Adr cells became worse (Figure 13C). The intracellular targeting drug delivery system achieved very good synergistic effects in destroying MDR cancer cells when MCF-7 / Adr cells were incubated with the combination nanocomplex, as evidenced by bio-TEM imaging, which revealed the worst cell apoptosis in MCF-7/Adr cells. The cell morphology showed decreased cell volume, shrunken cytoplasm, thickened plasma membrane, and lysed organelles (Figure 13D).

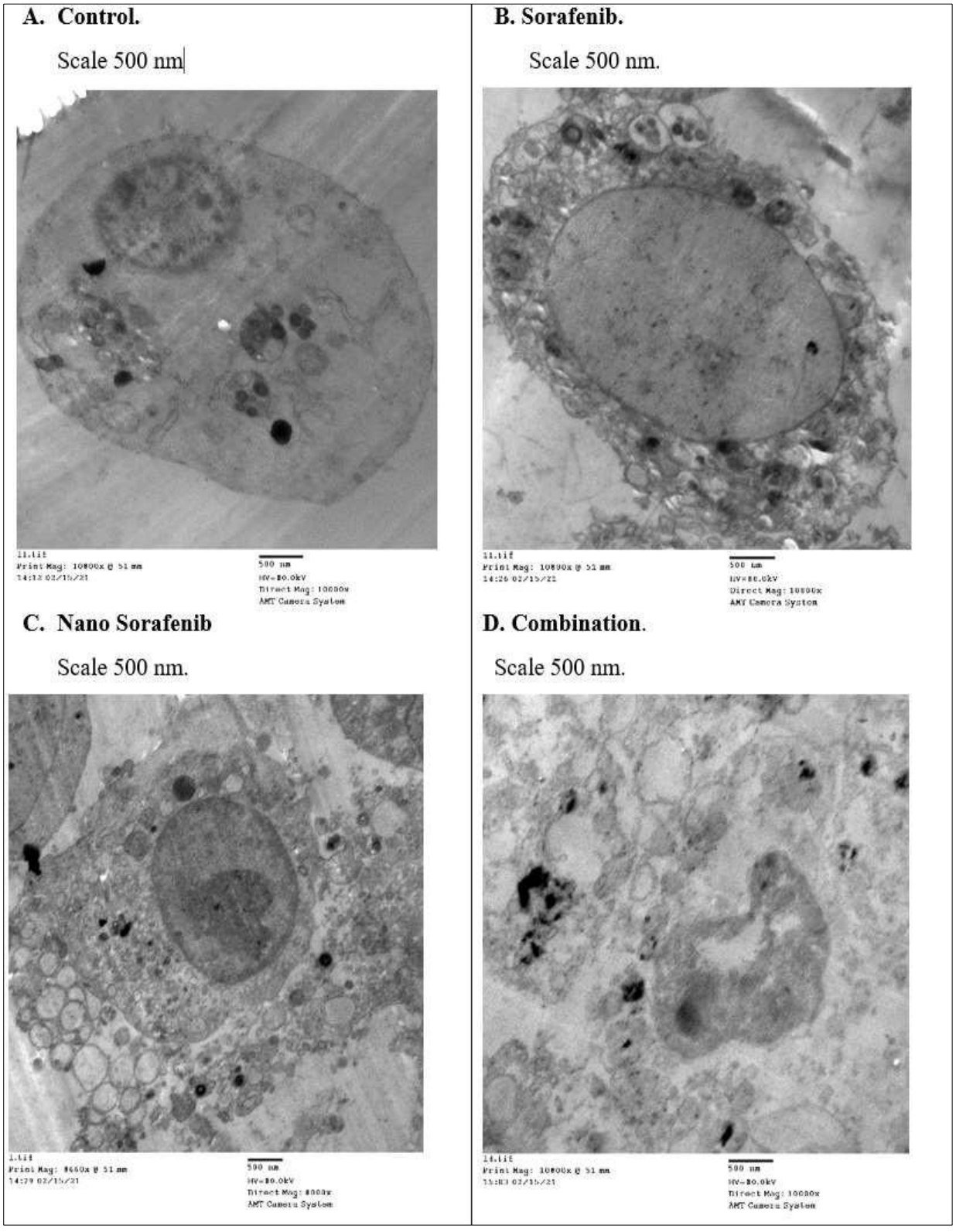

Figure 13. TEM micrographs of the ultrastructural characteristics of MCF-7/Adr cells treated with Sor, nano-Sor, and combination for 48 hours.

4. Discussion:

The aim of this study is to evaluate the importance of CsNPs-Sor-FA to enable active targeting and overcoming of MDR in breast cancer cells through activation of apoptotic signaling pathways. The impact of apoptosis on diseases such as cancer highlights the need for regulators involved in programmed cell death. An increase in the permeability of the mitochondrial outer membrane is decisive for apoptotic cell death. Mitochondrial membrane permeability is directly controlled by the Bcl-2 family, which regulates the formation of pores that transport apoptotic proteins to the outer membrane of mitochondria. However, the detailed molecular mechanisms are not yet fully understood. Mitochondrial cytochrome c is released through the intrinsic mechanism of apoptosis, which then triggers the activation of caspase-9 and caspase-3. After Cytochrome-c is released, the kinetics of caspase activation vary depending on the type of cell (Akl et al. 2014; Pfeffer and Singh 2018).

In the present study, the combination activated the intrinsic pathway in human breast cancer MCF7/Adr cells rather than Sor or nano-Sor by causing down-regulation of Bcl-2 and up-regulation of p53, which activate the mitochondrial signaling pathway. p53 promotes apoptosis mainly through direct activation of pro-apoptotic BH3 protein transcription. PUMA, which belongs to the Bcl-2 protein family, is a pro-apoptotic protein. The expression of PUMA is controlled by p53. PUMA plays a role in both p53-dependent and p53-independent cell death. By acting through members of the multidomain Bcl-2 family, PUMA works as a proximal signaling molecule that delivers death signals to mitochondria, where it causes mitochondrial malfunction and activates the caspase enzyme.

The results of this study showed that mitochondrial activation was accompanied by up-regulation of cytochrome c released from the intermembrane space of mitochondria into the cytosol. Cytochrome-c, apoptotic protease activating factor 1 (APAF-1), procaspase-9, and dATP together form the apoptosome, resulting in the activation of caspase-9, which activates executor caspase-3. Executioner caspases rapidly degrade proteins, causing cell apoptosis. These results were consistent with previous studies showing mitochondrial pathway-induced apoptosis in MCF7/Adr human breast cancer cells using Sor and another drug called resveratrol, which induces upregulation of p53, caspase 9, caspase 3, and downregulation of Bcl-2 (Mondal and Bennett 2016).

Resistance to apoptosis is one of the most common causes of cancer treatment failure (Kobayashi et al. 2007). The chemotherapeutic approach may become obsolete due to the development of chemoresistance. Breast cancer cells usually develop multidrug resistance after exposure to cytotoxic drugs. The mechanisms of MDR are very complicated. However, the most common cause of MDR in clinics is the overexpression of a transmembrane glycoprotein called P-glycoprotein (P-gp). P-gp promotes the efflux of internalized factors, leading to a reduction in the intracellular accumulation of cytotoxic substances in tumor cells, such as B. Adriamycin (Li et al. 2019). Alternatively, Nrf2, according to recent findings, regulates the cytoprotective response, which is focused on the activation of detoxification mechanisms in response to electrophilic/oxidative stress or xenobiotic stress. Importantly, it is known that sustained Nrf2 signaling in cancer cells can play a role in organizing the "programmed" pro-oncogenic process, ultimately promoting the progression of malignancies and the development of resistance to treatment with poor clinical outcomes. In breast cancer patients, increased Nrf2 expression leads to a decrease in overall survival

(Almeida et al. 2020). On the resistance question, our study found that Sor, nano-Sor, and combinations reduced Nrf2 expression in MCF7/Adr. It is interesting to note that the combination was more effective than that of Sor and nano-Sor. These results are consistent with those observed in a previous study in which Sor inhibited Nrf2 expression in the 5-FU-induced 5-FU-resistant HCC cell line Bel-7402/5-FU (Zhou et al. 2013).

Our results further support the idea that drug delivery systems based on nanocarriers, such as nanoparticles, have some advantages over traditional drug delivery systems. This is due to the ability of the host nanodrug delivery system to protect the drug from premature degradation and interaction with nontarget biological environments such as proteins, lipids, and other biological substances. Furthermore, many studies have been performed on the delivery of anticancer drugs using highly biocompatible Cs nanocarriers conjugated with folic acid to improve drug absorption in specific areas, such as tumors (Ruman et al. 2021). CsNPs are a good carrier to deliver the anticancer drug Sor in vivo with minimum toxicity (Joseph et al. 2021), while the use of FA as a targeting component may allow targeted delivery to folate receptors on the surface of breast cancer cells (John et al. 2017). Incorporation of the drug into breast cancer cells is significantly increased due to this target specificity. It was proposed that the expression of FR on the surface of tumor cells could specifically bind to folate-coupled delivery mechanisms and be carried intracellularly by clathrin-mediated endocytosis.

There are intracellular and external signals that can cause apoptosis. Intrinsic and extrinsic mechanisms related to signaling types lead to apoptosis. These are also known as the mitochondrial signaling pathway and the death receptor pathway (Pfeffer and Singh 2018). The extrinsic apoptotic pathway is induced when a death ligand such as TNF binds to TNFR1, the classic death receptor. The intracellular death domain of these death receptors interacts with adapter proteins like TRADD (TNF receptor-associated death domain). The death-inducing signaling complex (DISC) is the name given to the complex formed when the death ligand binds to the death receptor, which provides a binding site for the adapter protein. The DISC then starts to assemble and activate Caspase 8. Activated caspase 8 is an initiator caspase that cleaves effector caspases such as caspase 3 to induce apoptosis (Wong, 2011). Our results clearly showed that after combination treatment, TNFR expression decreased while caspase-8 increased rather than Sor or nano-Sor, suggesting that the extrinsic apoptotic pathway was also activated. Previous studies have shown that Sor stimulates extrinsic and intrinsic apoptotic pathways in osteosarcoma cells, leading to increased expression of cleaved caspases 3, 8, and 9 (Wu et al. 2021).

By evaluation of the plasma membrane's permeability to a fluorescent dye that is typically impermeable, such as the PI-DNA-binding dye, necrosis can be identified. Using fluorescently labeled annexin V, externalization of phosphatidylserine to the cell membrane can be used to identify apoptosis. In the current study, the Annexin V/PI-based apoptosis assay also showed that apoptosis and necrosis were triggered more in the combination-treated cells than in those treated with Sor or nano-Sor. What is surprising is that the dominant cell death mechanism in Sor or nano-Sor was apoptosis with 32.0% and 38.2%, respectively, while in combination the dominant mechanism was necrosis with 74.6%. As mentioned above, p53 is a protein found in the cell nucleus that plays a key role in controlling cell death and cell division. Numerous cellular stressors, such as DNA damage, hypoxia, and mitogenic oncogenes,

activate p53. Cells with extensive DNA damage are encouraged to undergo cell cycle arrest by activated p53 to allow DNA apoptosis or repair. Considering the cell cycle, a previous study showed that Sor treatment reduced the proliferation of MDA-MB-231 and MCF7 breast cancer cells by stopping the cell cycle in the G1 phase (Dattachoudhury et al. 2020). This report disagrees with our findings. The current results show that Sor, nano-Sor, and the combination arrest cells in the S phase of the cell cycle. In addition, our results showed that the combination produced more fragmented DNA than Sor and nano-Sor, indicating that the combination was more effective than Sor and nano-Sor. This report was consistent with a previous report showing that sor-induced DNA fragmentation occurred in PLC/PRF/5 and HepG2 HCC cell lines (Liu et al. 2006).

Regarding toxicity, in this study, nanosomal Sor reduced the viability of MCF7 / Adr cells more than Sor or combination treatments. However, the combination showed the highest selectivity index compared to their individual treatments in vitro. These results are in agreement with previous studies showing that Sor inhibits cell proliferation in PLC/PRF/5-HCC and HepG2 cell lines (Liu et al. 2006). Furthermore, due to their high drug loading capacity, low cytotoxicity on normal cells, and decreased viability of HepG2 and HT29 cell lines, both the CsNPs-Sor and CsNPs-Sor-FA nanodrug delivery systems show promise for liver and colon cancer (Ruman et al. 2021).

An in vitro transmission electron microscope allows direct observation of morphology and structural changes in MCF7/Adr cells. Sor, nano-Sor, or the combination caused morphological alterations in treated cells that were indicative of apoptosis, such as membrane blebbing, cell shrinkage, mitochondrial condensation, and nuclear condensation. These findings supported earlier research suggesting that sorafenib promotes the rate of apoptosis in breast cancer (Wilhelm et al., 2004). Furthermore, the targeted drug delivery system enhances this effect. Our preliminary results suggest that this combination could be very beneficial in treating human breast cancer by increasing potency and effectiveness while minimizing side effects. As a result, nanoparticle combinations have provided a promising delivery vehicle for breast cancer. However, further studies on the potential of nanoparticles, such as in vivo studies, are needed to investigate the effectiveness of synthesized nanoparticles.

Conclusion:

Compared to free Sor and nano-Sor, the combination nanoparticles showed impressive anticancer effects in the cell lines MCF7 and Adr. This nanodrug delivery method showed extremely promising behavior for breast cancer due to its potent anticancer activity, high drug loading capacity, and low cytotoxicity. The combination of nanoparticles inhibits cell cycle progression and Nrf2 activity, activates the mitochondrial signaling pathway and the death receptor pathway, and causes apoptosis in MCF7 / Adr cells from breast cancer. DNA fragmentation, activation of P53, Caspases 9, 8, and 3, Cytochrome-c release, TNFR production, and suppression of Bcl-2 are all significantly influenced by combined therapy. Our findings suggest that the combination could be very useful in the treatment of human breast cancer. The limitation of this study is that we studied the effect of the combined treatment (CsNPs-Sor-FA) on only one type of breast cancer cell line, and there are other different types of breast cancer cell line such as Evsa-T, Hs578T, and ZR-75-1.

Acknowledgements

The authors are grateful to all members of Materials Science and Nanotechnology Dept., Faculty of Postgraduate Studies for Advanced Sciences (PSAS), Beni-Suef University Egypt for supporting the preparation of the nanomaterials. Also, all members at Central Laboratory for Characterization

Ethics approval and consent to participate.

Not applicable.

Consent for publication.

All authors agreed with the content of the manuscript and agreed to submit the manuscript.

Availability of data and material

The data supporting the findings of this study are available from the corresponding author, Dr. Ahmed Nabil, upon request.

Funding

The authors have no affiliation with any organization with a direct or indirect financial interest in the subject matter discussed in the manuscript. The standing research paper was maintained through individual funding.

Authors contribution:

Asmaa Hassan: Investigation, Methodology, Formal analysis, Writing - review & editing. **Ahmed Nabil:** Supervision, Resources, Funding acquisition, Project administration, Conceptualization, Investigation, Methodology, Data curation, Formal analysis, Validation, Visualization, Writing - original draft, Writing - review & editing. **Islam S. Ali:** Investigation, Methodology, Formal analysis, & Writing – Original Draft. **Mariam Elwan:** Investigation, Methodology. **Zeinab Reyd:** Methodology & Writing - review & editing. **Osama M. Ahmed:** Supervision, Formal analysis, Resources, Project administration & Writing - review & editing. **Ahmed A. G. El-Shahawy:** Supervision, Resources, Funding acquisition, Project administration, Conceptualization, Investigation, Methodology, Data curation, Formal analysis, Validation, Visualization, Writing - original draft, Writing - review & editing.

References:

Abdel-Motaal M, Nabil A. Biological activity of some newly synthesized hydrazone derivatives derived from (dicyclopropylmethylene) hydrazone. Eur Chem Bull 2018;7(10):280-287.

Akl H, Vervloessem T, Kiviluoto S et al. A dual role for the anti-apoptotic Bcl-2 protein in cancer: mitochondria versus endoplasmic reticulum. Biochimica et biophysica acta (BBA)-molecular cell research 2014; 1843(10):2240-52.

Almeida M, Soares M, Ramalhinho AC et al. The prognostic value of NRF2 in breast cancer patients: A systematic review with meta-analysis. Breast Cancer Res Treat 2020;179:523-32.

Amin BH, Ahmed HY, El-Aziz MM. In Vitro Anticancer Activity of Fungal Secondary Metabolites of Stemphylium Lycopersici. N Egypt J Microbiol 2018;50:80-97.

Chae SY, Jang MK, Nah JW. Influence of molecular weight on oral absorption of water soluble chitosans. J Control Release 2005;102(2):383-394.

Dattachoudhury S, Sharma R, Kumar A et al. Sorafenib Inhibits Proliferation, Migration and Invasion of Breast Cancer Cells. Oncol 2020;98(7):478-486.

Ebadi M, Buskaran K, Bullo S et al. Pastorin, Synthesis and Cytotoxicity Study of Magnetite Nanoparticles Coated with Polyethylene Glycol and Sorafenib-Zinc/Aluminium Layered Double Hydroxide. Polymers 2020;12(11):2716.

Fraguas-Sánchez AI, Fernández-Carballido A, Simancas-Herbada R et al. CBD loaded microparticles as a potential formulation to improve paclitaxel and doxorubicin-based chemotherapy in breast cancer. Int J Pharm 2020;574:118916.

Fumarola C, Caffarra C, La Monica S et al. Effects of sorafenib on energy metabolism in breast cancer cells: Role of AMPK-mTORC1 signaling. Breast Cancer Res Treat 2013;141(1):67-78.

Ghosheh OA, HoudI AA, Crooks PA. High performance liquid chromatographic analysis of the pharmacologically active quinones and related compounds in the oil of the black seed (Nigella sativa L.). J Pharm Biomed Anal 1999;19(5):757-62.

Guido S, Joseph T. Effect of chemically different calcium antagonists on lipid profile in rats fed on a high fat diet. Indian J Exp Biol 1992;30(4):292-4.

John AA, Jaganathan SK, Ayyar M. Folic acid decorated chitosan nanoparticles and its derivatives for the delivery of drugs and genes to cancer cells. Curr Sci 2017;113(8):1530-1542.

Joseph JJ, Sangeetha D, Gomathi T et al. Formulation and evaluation of the anticancer drug, sorafenib. Trends in Biomaterials and Artificial Organs 2021;35(4):336-338.

Katz A, Nambi SS, Mather K et al. Quantitative insulin sensitivity check index: a simple, accurate method for assessing insulin sensitivity in humans. J Clin Endocrinol Metab 2000;85(7):2402-10.

Keating GM. Sorafenib: A Review in Hepatocellular Carcinoma. Target Oncol 2017;12(2):243-253.

Khan MA, Zafaryab M, Mehdi SH, et al. Characterization and carboplatin loaded chitosan nanoparticles for the chemotherapy against breast cancer in vitro studies. Int J Biol Macromol 2017;97:115-122.

Kobayashi H, Mochizuki H, Sugihara K et al. Characteristics of recurrence and surveillance tools after curative resection for colorectal cancer: a multicenter study. Surgery 2007;141(1):67-75.

Li JM, Zhang W, Su H et al. Reversal of multidrug resistance in MCF-7/Adr cells by codelivery of doxorubicin and BCL2 siRNA using a folic acid-conjugated polyethylenimine hydroxypropyl-β-cyclodextrin nanocarrier. Int J Nanomedicine 2015;10:3147-3162.

Liu L, Cao Y, Chen C et al. Sorafenib blocks the RAF/MEK/ERK pathway, inhibits tumor angiogenesis, and induces tumor cell apoptosis in hepatocellular carcinoma model PLC/PRF/5. Cancer Res 2006;66(24):11851-11858.

Li Y, Sun Y, Tang T et al. aris saponin VII reverses chemoresistance in breast MCF-7/Adr cells. J Ethnopharmacol 2019;232:47-54.

Li Y, Wang M, Zhi P et al. Metformin synergistically suppress tumor growth with doxorubicin and reverse drug resistance by inhibiting the expression and function of P-glycoprotein in MCF7/ADR cells and xenograft models. Oncotarget 2018;9(2):2158–2174.

Matthews DR, Hosker JP, Rudenski AS et al. Homeostasis model assessment: insulin resistance and beta-cell function

from fasting plasma glucose and insulin concentrations in man. Diabetologia 1985;28:412–419.

Mittal A, Mahala N, Krishna KV et al. Calcium chloride linked camel milk derived casein nanoparticles for the delivery of sorafenib in Hepatocarcinoma cells. BIOCELL 2021;46:(1), 127-136.

Mondal A, Bennett LL. Resveratrol enhances the efficacy of sorafenib mediated apoptosis in human breast cancer MCF7 cells through ROS, cell cycle inhibition, caspase 3 and PARP cleavage. Biomed Pharmacother 2016;84:1906-1914.

Nguyen VD, Min HK, Kim CS et al. Folate receptor-targeted liposomal nanocomplex for effective synergistic photothermal-chemotherapy of breast cancer in vivo. Colloids Surfaces B Biointerfaces 2019;173:539-548.

Pfeffer CM, Singh ATK. Apoptosis: A target for anticancer therapy. Int J Mol Sci 2018;19(2).

Prathima MB, Reshma S, Sushith S et al. Estimation of glycated haemoglobin by nephelometry, ion exchange resin and high-performance liquid chromatography: a cross-sectional study. J Clin Diagnostic Res 2020;14(9):BC01–BC04.

Ruman U, Buskaran K, Pastorin G et al. Synthesis and characterization of chitosan-based nanodelivery systems to enhance the anticancer effect of sorafenib drug in hepatocellular carcinoma and colorectal adenocarcinoma cells. Nanomaterials 2021;11(2):497.

Senapati S, Mahanta AK, Kumar S et al. Controlled drug delivery vehicles for cancer treatment and their performance. Signal Transduct Target Ther 2018;3(1):1-19.

Shahverdi AR, Shahverdi F, Faghfuri E et al. Characterization of Folic Acid Surface-Coated Selenium Nanoparticles and Corresponding In Vitro and In Vivo Effects Against Breast Cancer. Arch Med Res 2018;49(1):10-17.

Shanmuganathan R, Edison TN, Lewis-Oscar F et al. Chitosan nanopolymers: An overview of drug delivery against cancer. Int J Biol Macromol 2019;130:727-736.

Tamilselvan N, Raghavan CV. Formulation and characterization of anti- Alzheimer's drug loaded chitosan nanoparticles and its in vitro biological evaluation. J Young Pharm 2015;7(1):28-35.

Tran P, Lee SE, Kim DH et al. Recent advances of nanotechnology for the delivery of anticancer drugs for breast cancer treatment. J Pharm Investig 2020;50(3):261-270.

Truong DH, Tran TH, Ramasamy T et al. Preparation and characterization of solid dispersion using a novel amphiphilic copolymer to enhance dissolution and oral bioavailability of sorafenib. Powder Technol 2015;283:260-265.

Waks AG, Winer EP. Breast Cancer Treatment: A Review. JAMA - J Am Med Assoc 2019;321(3):288–300.

Wang D, Romer F, Connell L et al. Highly Flexible Silica/Chitosan Hybrid Scaffolds with Oriented Pores for Tissue Regeneration. J Mater Chem B 2015;3:7560–7576.

Wilhelm SM, Adnane L, Newell P et al. Preclinical overview of sorafenib, a multikinase inhibitor that targets both Raf and VEGF and PDGF receptor tyrosine kinase signaling. Mol Cancer Ther 2018;7(10):3129-3140.

Wilhelm SM, Carter C, Tang L et al. BAY 43-9006 exhibits broad spectrum oral antitumor activity and targets the RAF/MEK/ERK pathway and receptor tyrosine kinases involved in tumor progression and angiogenesis. Cancer Res 2004;64(19):7099-109

Wong RSY. Apoptosis in cancer: From pathogenesis to treatment. J Exp Clin Cancer Res 2011;30(1):1-14.

Wu CH, Lin KH, Fu BS et al. Sorafenib induces apoptosis and inhibits NF-κB-mediated anti-apoptotic and metastatic potential in osteosarcoma cells. Anticancer Res 2021;41(3):1251-1259.

Zhou S, Ye W, Duan X et al. The noncytotoxic dose of sorafenib sensitizes Bel-7402/5-FU cells to 5-FU by down-regulating 5-FU-induced Nrf2 expression. Dig Dis Sci 2013;58:1615-26.